Desalination and Water Treatment
www.deswater.com

doi: 10.5004/dwt.2019.23725

150 (2019) 136–145
May

Preparation, characterization, and catalytic activity of a magnetic photocatalyst (Fe_3O_4@TiO_2)

Ulisses Magalhães Nascimento[a,*], Laudemir Carlos Varanda[b], Eduardo Bessa Azevedo[c]

[a]*Universidade Federal do Maranhão (UFMA), Centro Ciências Exatas e Tecnologia, Departamento de Tecnologia Química (DETEQ), Núcleo de Combustíveis, Catálise e Ambiental (NCCA), Avenida dos Portugueses, 1966 – Bacanga, São Luís/MA Zip Code: 65080-805, Brazil, Tel. +55 98 3272 8244; email: ulisses.nascimento@ufma.br*
[b]*Universidade de São Paulo (USP), Instituto de Química de São Carlos (IQSC), Departamento de Físico-Química (DFQ), Grupo de Materiais Coloidais (GMC), Avenida Trabalhador São-Carlense, 400 – Centro, São Carlos/SP Zip Code: 13560-970, Brazil, Tel. 55 16 3373 8102; Fax: 55 16 3373 9951; email: lvaranda@iqsc.usp.br*
[c]*Universidade de São Paulo (USP), Instituto de Química de São Carlos (IQSC), Departamento de Química e Física Molecular (DQFM), Laboratório de Desenvolvimento de Tecnologias Ambientais (LDTAmb), Avenida Trabalhador São-Carlense, 400 – Centro, São Carlos/SP Zip Code: 13560-970, Brazil, Tel. 55 16 3373 9962; Fax: 55 16 3373 9975; email: bessa@iqsc.usp.br*

Received 16 August 2018; Accepted 31 December 2018

ABSTRACT

Magnetic core-shell photocatalytic microparticles were synthesized by a simple precipitation (α-Fe_2O_3), heterocoagulation (α-Fe_2O_3@TiO_2), and magnetization (Fe_3O_4@TiO_2) methodology. Their specific surface area, average size, and average pore size were 202 ± 5.0 m^2 g^{-1}, 1.5 μm, and 7.0 nm, respectively. The microparticles photocatalytic activity was assessed using Acid Blue 9 (AB9) as a model-pollutant. By using 1.0 g photocatayst L^{-1}, 60% of the initial color of a 25 mg AB9 L^{-1} was removed in 120 min (whereas only a 14% color removal was observed by direct photolysis with a medium pressure mercury vapor lamp). The particles were magnetically separated from the dye solution (50 mL) in 2 min using an ordinary magnet. After ten reuse cycles, no perceivable photocatalytic activity losses occurred. Therefore, the synthesized microparticles behaved as a feasible magnetically-recyclable photocatalyst, at least regarding AB9 degradation.

Keywords: AOP; TiO_2; Magnetic photocatalyst; Core-shell; Acid blue 9

1. Introduction

Although, biological processes deliver the best results for the removal of high organic loads from wastewaters with large flow rates, they are markedly inefficient toward pollutants presenting low biodegradability and/or ecotoxicity [1].

To fill in this gap, advanced oxidation processes (AOPs) are a feasible choice. They are based on the "in situ" generation of hydroxyl radicals (•OH), the second best oxidant in nature [2,3]. AOPs have been efficiently used for several environmental applications: water and wastewater treatment, disinfection, air purification, soil remediation, and the treatment of volatile organic compounds [4].

The most studied AOP is heterogeneous photocatalysis with titanium dioxide (TiO_2) as the photocatalyst. That is a solid with low cost, low ecotoxicity, high photo-stability, and it can be used in a wide range of pHs [5]. However, TiO_2 also has some disadvantages, such as: it is only UV-excited and requires an additional unit operation (e.g. filtration or centrifugation) for reuse purposes [6].

To overcome that last drawback, one could use magnetic photocatalysts, as they would be easily separated from the reaction medium with the aid of a magnet. One of those

* Corresponding author.

photocatalysts, Fe_3O_4@TiO_2 (core: magnetite; shell: titanium dioxide), consists of particles with magnetic nuclei coated with a photoactive substance. Recently, good results have been reported for a wide range of applications, such as: degradation of dyes and other organic pollutants [7–12], destruction of tumor cells [13,14], inhibition and destruction of pathogenic bacteria [15], and other biotechnological applications [16–19].

The aim of this study was then to apply a simple procedure for synthesizing a magnetic photocatalyst (Fe_3O_4@TiO_2), with high specific surface area, good photocatytic activity (when compared with Evonik's TiO_2 P25), and high reuse rates.

A water-soluble triarylmethane dye (Acid Blue 9, C.I. 42090 and Fig. 1) was chosen as a model-pollutant to assess the synthesized particles photocatalytic activity due to:

- It is used by several (textile, food, pharmaceutical, etc.) industries [20–22].
- It is the major dye in the product Aquashade®, a pre-emergent pesticide widely used for aquatic plants growth control [23–25].
- It is a valuable dye tracer for visualizing water flow patterns in soils [26].
- It is photo-stable, linked to mutagenic and bioaccumulative effects, and it presents low biodegradability [27–29].

2. Materials and methods

2.1. Synthesis of hematite (α-Fe_2O_3) sub-micro particles

Hematite sub-micro particles were prepared by the precipitation method [30]. The pH of aqueous iron(III) chloride hexahydrate (500 mL, 0.01 mol L^{-1}) was set to 10.5 with aqueous sodium hydroxide (0.5 mol L^{-1}), under continuous stirring. Protons release, during hydrolysis, may take place either by olation or oxolation [31]. The generated oxyhydroxide, as a gelatinous black precipitate, was decanted and the supernatant discarded.

The precipitate was washed with distilled water until its pH decreased to 9.3. Next, aqueous hydrochloric acid (10 mL, 1.0 mol L^{-1}) were added to a suspension of the precipitate in water (250 mL) to avoid the formation of other iron phases, but hematite. The suspension was made up to 500 mL with distilled water and aged for 48 h at 105°C in a Roux flask (1,000 mL) [32,33].

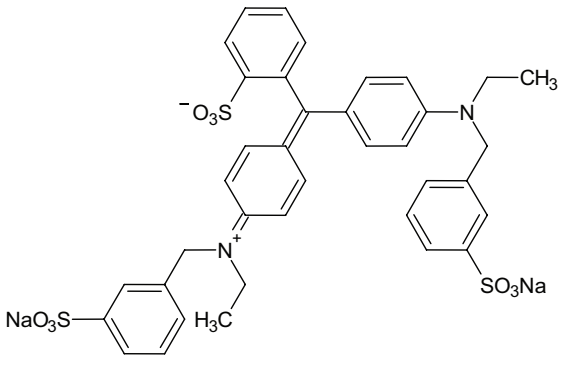

Fig. 1. Model-pollutant: Acid Blue 9 (triarylmethane dye, C.I. 42090).

Finally, a metallic-red suspension was formed. Its pH was set to 6.0 with aqueous sodium hydroxide (0.5 mol L^{-1}), under continuous stirring, in order to expedite hematite sub-micro particles precipitation from suspension. The sub-micro particles were filtered, thoroughly washed with distilled water until no turbidity was observed upon adding diluted aqueous silver nitrate to the wash water, and dried at 50°C for 2 h.

2.2. Functionalization of hematite sub-micro particles

The functionalization was performed in two steps: (a) TiO_2 coating of the synthesized sub-micro particles by heterocoagulation [34] and (b) phase transformation, from α-Fe_2O_3 to Fe_3O_4 (magnetization), by controlled heating under reducing atmosphere [35].

2.2.1. TiO_2 coating

$TiCl_4$ (99%, 100 mL) was transferred to a beaker. Next, a certain volume of distilled water was slowly added, under continuous stirring, to make approximately 1,000 mL of solution. The temperature of reagents and glassware was maintained under 0°C [36]. During hydrolysis, it was formed a yellowish precipitate of $TiO(OH)_2$ (unstable) and then a yellowish solution of $TiOCl_2$ [37]. The Ti^{4+} concentration in that solution (stock solution) was measured by Inductively Coupled Plasma/Optical Emission Spectrometry (ICP-OES): 1.82 mol L^{-1}.

According to the desired Ti^{4+} concentration in a particular experiment, 100 mL of the stock solution were transferred to a three-neck round-bottom flask and diluted with distilled water, under continuous stirring. The diluted solution pH was raised to approximately 13 by adding aqueous NaOH (2.5 mol L^{-1}). Next, 100 mg of sub-micro particles were added to the flask and carbon dioxide bubbled until pH decreased to 6.8. At that point, a layer of titanium hydroxides and/or oxyhydroxides precipitates on the hematite sub-micro particles [34]. The TiO_2-coated sub-micro particles were filtered and washed with distilled water (to remove impurities), dried, and calcined at 500°C for 2 h to consolidate the TiO_2 layer (anatase).

2.2.2. Magnetization

The coated (TiO_2) hematite sub-micro particles were inserted in a tubular furnace at 400°C for 1 h. The reducing atmosphere was provided by a H_2 flux with a flow rate of 22 mL min^{-1}. During that process, the sub-micro particles core becomes magnetic (by converting α-Fe_2O_3 into Fe_3O_4), without any changes to the TiO_2 shell.

2.3. Sub-micro particles characterization

2.3.1. X-ray diffraction (XRD)

A Rigaku-Denki (Rint2000) powder diffractometer with a conventional X-ray generator was used (CuKα, l = 1.5418 Å). The scanning angle was varied between 20° and 70°; the scanning speed was 0.010° s^{-1} in 2θ.

The obtained diffratograms were compared with standard ones available in the International Center for Diffraction Data (ICDD) libraries (CD-ROM, 1998 JCPDS, PCPDFWIN v.2.01 crystallographic cards collection).

2.3.2. Electrophoretic mobility analyses (isoelectric point and zeta potential)

According to the International Union of Pure and Applied Chemistry, [38] the isoelectric point (IEP) is "The pH value at which the net electric charge of an elementary entity [of a particle] is zero. pI is a commonly used symbol for this kind-of-quantity. It should be replaced by pH(I) because it is a pH determined under that particular condition.". On the other hand, the Point of Zero Charge (PZC) is obtained "(…) when the surface charge density (of a particle) is zero. It is a value of the negative logarithm of the activity in the bulk of the charge-determining ions". When there is no specific adsorption of ions on a particle surface, the pH(I) and the PZC are the same.

The PZC, size distribution, and additional information about the sub-micro particles coating were obtained by electrophoretic mobility (pH 2–9) with the aid of a Zetasizer Nano Z (Malvern). The synthesized sub-micro particles (5–10 mg) were suspended in KNO_3 10^{-2} mol L^{-1} (100 mL). The desired pH in each experiment was achieved by adding diluted KOH or HNO_3.

2.3.3. Field emission gun scanning electron microscopy (FEG-SEM) and energy dispersive X-ray spectrometry

The polycrystalline aggregates morphology was observed in a Philips XL–30 FEG system with an acceleration voltage of 10–25 kV and magnification of 25,000–1,00,000x.

A small amount of sub-micro particles was suspended in anhydrous ethanol and sonicated for 5 min. That suspension was then added dropwise to an aluminum support. That support was then dried at 50°C for 1 h. After cooling down to room temperature, it was metallized with gold.

The semi-quantitative composition of the sub-micro particles (titanium, oxygen, and iron) was determined by EDS, with an acceleration voltage of 20–30 kV.

2.3.4. Specific surface area and pore size distribution

Adsorption/Desorption isotherms were obtained in a Quantachrome equipment, model Nova 1000, using nitrogen as the inert gas. The sub-micro particles specific surface area was calculated by the Brunauer-Emmet-Teller (BET) method. Samples were previously degased at 150°C for 2 h.

The sub-micro particles pores volume distribution was calculated by applying the Barret-Joyner-Halenda (BJH) method to the desorption isotherms [39].

2.3.5. Magnetic characterization

It was accomplished using an MPMS-5S Quantum Design SQUID (Superconducting Quantum Interference Device) at 300 K and with an applied magnetic field above 10 kOe (1 *T*). Magnetic saturation (M_S), coercivity (H_C), and remanence (B_R) values were obtained by hysteresis loops at room temperature. Samples were packed in a plastic tube.

Verwey and Curie temperatures were estimated by zero-field cooled and field cooled (ZFC and FC, respectively) magnetization curves (5–300 K) [40,41].

2.4. Photocatalytic activity tests

2.4.1. Reactor characterization

The experiments were performed in a 250 mL cylindrical borosilicate reactor, kept at 25°C ± 2°C (Fig. S1(a)). The suspension was irradiated with a 250 W medium pressure mercury vapor lamp (Philips HPL-N), whose outer bulb was removed. The lamp was positioned 15 cm above the liquid layer. Its emission spectrum was measured by a Stellarnet EPP2000C-50 spectroradiometer also at 15 cm away from the lamp (Fig. S1(b)).

2.4.2. Experimental procedure

In all experiments, 50 mL of a 25 mg L^{-1} Acid Blue 9 (AB9) solution was used. First, to the reactor already containing the dye solution, a pre-determined catalyst amount (0.3 or 1.0 g L^{-1}) was added. Next, the suspension was sonicated (Odontobrás, 20 Hz) for 20 min and maintained under magnetic stirring throughout each experiment. The suspension pH was adjusted with diluted H_2SO_4 (Synth) or NaOH (Quemis), accordingly (3.0 or 8.0). Air was bubbled and the reactor was kept in the dark to attain the adsorption equilibrium. Then, the reactor was irradiated for 60 min. Finally, the catalyst was magnetically separated (with an ordinary magnet) and the effluent was vacuum-filtered through 0.45 μm pore-size cellulose nitrate membranes.

The suspension "concentration" and pH were set according to a 2^2 factorial design, with four repetitions of the central point, conceived to study these variables (factors) with a minimum number of statistically validated experiments [42].

2.4.3. Color removal

The visible absorption spectra (400–700 nm) of treated samples were obtained by a Varian Cary Win UV Scan Application spectrophotometer. Then, OriginPro® 8.0 software was used to numerically integrate the area below those spectra. Calculated areas were used as an indirect measure of the samples color.

3. Results and discussions

3.1. Structural and morphological characterization of hematite sub-micro particles

A well-defined hematite phase, with good crystallinity was obtained (Fig. 2). All of the observed peaks in the diffractogram were an almost perfect match to the diffraction lines of romboedric hematite (α-Fe_2O_3, JCPDS # 33–0664).

Fig. S2(a) presents a micrograph taken showing agglomerates formed by impurities-free, rounded hematite particles with a well-defined phase. Additionally, they presented a narrow size distribution, centered at approximately 155 nm (Fig. S2(b)).

Particles size is closely related to their synthesis pH. When the pH value is similar to the pH(I) one, hematite particles of around 8.0 μm are obtained; however, in extremely acidic or basic conditions, particles of approximately 100 nm are formed [43]. Surface charges decrease, when pH ≅ pH(I), resulting in very weak repulsive electrostatic forces;

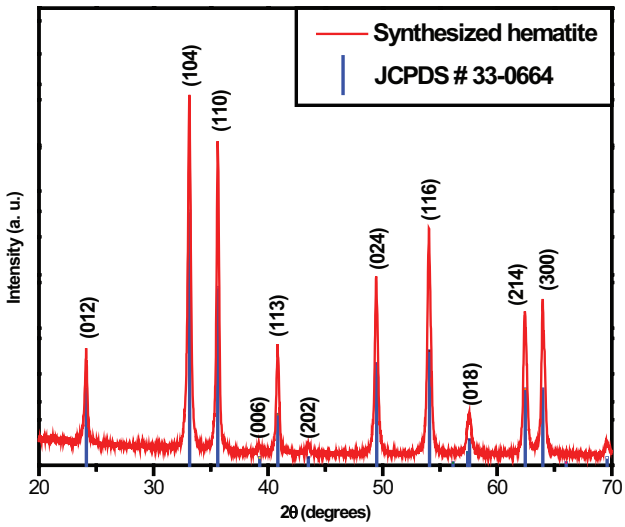

Fig. 2. Diffractogram of the synthesized hematite sub-micro particles by precipitation.

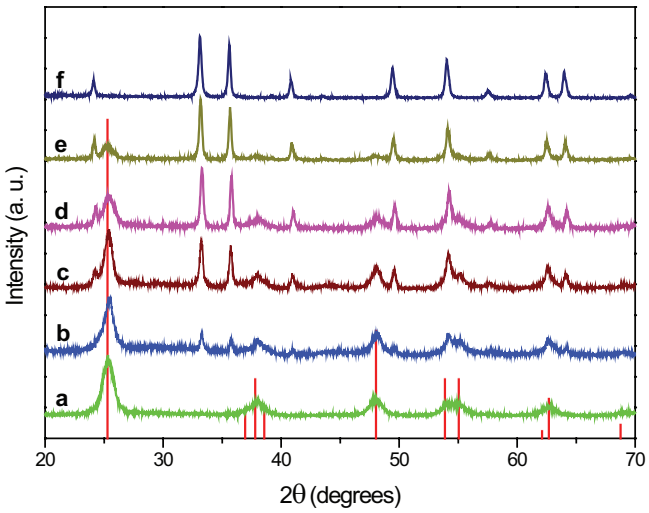

Fig. 3. Diffractograms of coated hematite cores by heterocoagulation with different Ti percentages (regarding the atomic ratio Fe:Ti) and calcined at 500°C for 2 h: (a) no cores (TiO_2 only); (b) Ti 90%; (c) Ti 70%; (d) Ti 50%; (e) Ti 30%; and (f) just cores (no TiO_2). Vertical red lines: TiO_2 (anatase, JCPDS # 21-1272).

therefore, attractive (van der Waals) forces predominate, increasing particles size.

The electrophoretic mobility analysis revealed a pH(I) of 9.0, which is within the usually reported range, 7.0 < pH(I) < 9.5, by other authors [44].

3.2. Functionalization of hematite sub-micro particles

3.2.1. TiO_2 coating

Although hematite could theoretically catalyze redox reactions [45,46], it should be coated with TiO_2 to improve its photocatalytic performance [47].

In order for the coating of (hematite) particles with the desired species (titania) to be generated, there must be a pH range within which they have opposite charges, so that electrostatic attraction becomes the driven force. That range is, for TiO_2 and Fe_2O_3, from 5.39 to 8.98, which happen to be their respective pH(I).

$FeCl_3$ concentration and hematite weight are key parameters for determining the Ti concentration that produces a material with the highest possible specific surface area and crystallinity.

Fig. 3 shows the diffractograms obtained for the hematite cores coated by heterocoagulation with different Ti percentages (regarding the atomic ratio Fe:Ti). After coating, all samples were calcined at 500°C for 2 h, so to dehydroxylate and consolidate the TiO_2 (anatase) layer [48]. One can observe that, in all tested conditions, adequate crystallinities were obtained, while maintaining the crystallographic characteristics of the hematite cores.

One can notice that when hematite cores were coated with 30% Ti, an ill-defined anatase phase was formed, what would probably impair the photocatalyst activity and the cores protection. On the other hand, samples coated with 90% Ti presented a considerable reduction in the cores characteristic peaks intensity, what would decrease the particles magnetization performance. Therefore, coatings with 30% or 50% Ti seemed to be the best choices in order to couple high crystallinity with magnetic properties, thus increasing the photocatalyst activity and recyclability.

A uniform TiO_2 shell upon Fe_2O_3 cores was attained, as depicted by the EDS mapping (Fig. S3). The results reinforce that heterocoagulation is an efficient strategy for functionalizing particles: appropriate specific surface areas were obtained without the need for surface changes on the cores to enhance their affinity for the shell.

3.2.2. Magnetization

Based on the previous results, this step was only performed with microparticles synthesized with 50% Ti.

Hematite (α-Fe_2O_3) can be magnetized by thermal treatment under reducing conditions, generating magnetite (Fe_3O_4), without changing the TiO_2 shell. Based on Lou and Archer's (2008) work, temperatures of 400°C and one hour of reducing atmosphere (H_2) were needed to completely change hematite into magnetite (Fig. S4). One can also notice the appearance of diffraction peaks at 2θ = 44.67° and 65.02°, probably assignable to the (110) and (200) planes of metallic iron (α-Fe, JCPDS N° 06–0696). That reduction to metallic iron may indicate that some cores were left uncoated.

3.2.3. Magnetic properties

In fact, magnetite is a compound oxide – iron(II,III) oxide – in which iron ions occupy interstices of a face-centered cubic structure formed by tetrahedral or octahedral oxygen atoms. This kind of structure promotes highly temperature-dependent magnetic properties [49], determined with the aid of a SQUID. Fig. 4 presents the FC and ZFC curves obtained in a 100 Oe external field. From those curves, two characteristic temperatures were estimated: (a) Verwey temperature (Tv) – the temperature in which the two approximately linear branches of the ZFC curve

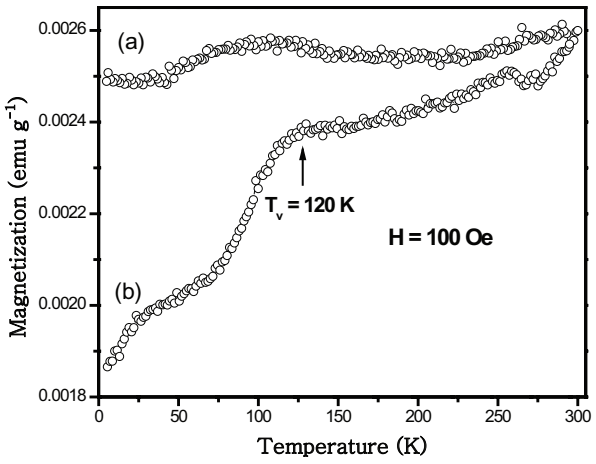

Fig. 4. Fe_3O_4@TiO_2 microparticles: (a) FC and (b) ZFC curves in a 100 Oe field.

intersect one another; and (b) Curie Temperature (Tc) – the temperature in which the FC and ZFC curves intersect one another. Verwey transitions occur due to a fast movement of electrons between ions Fe(II) and Fe(III). Those sometimes structural transitions may result in magnetic properties changes of the desired material [41].

In temperatures greater than T_v, Fe_3O_4@TiO_2 is paramagnetic; otherwise, below T_v, it is ferrimagnetic. Within the studied range, T_v was not observed, which means that the synthesized photocatalyst has, at room temperature, spontaneous magnetization.

The Fe_3O_4@TiO_2 photocatalyst magnetization (M) against an external applied magnetic field (H) was measured at 300 K (Fig. S5). The hysteresis loop in the $M \times H$ curve indicates that the synthesized photocatalyst is ferrimagnetic. Measured M_S, H_C and B_R were 0.20 emu g^{-1} (0.20 A m^2 kg^{-1}), 48.57 Oe (3,865 A m^{-1}), and 0.005 emu g^{-1} (0.005 A m^2 kg^{-1}), respectively. Those low magnetization values are in accordance with the weight of magnetite that composes the photocatalyst. Moreover, when non-magnetic materials (like TiO_2) coat magnetic particles, a passivation layer may be formed [41,49,50]. Those magnetic properties allowed the photocatalyst to be magnetically separated within 2.0 min.

3.3. Fe_3O_4@TiO_2 characterization

Micrographs revealed particles with similar features: micrometric dimensions, rugged surfaces and irregular, raspberry-like shapes (Fig. 5(a)). Although, hematite sub-micro particles were synthesized, core-shell microparticles were produced when they were coated. That was due to the cores agglomeration before the coating was completed. Afterwards, several layers of TiO_2 were yet deposited [51].

The measured specific surface area of the microparticles was 202 ± 5.0 m^2 g^{-1}, quite bigger than the one of Evonik's P25 (≅50 m^2 g^{-1}). The microparticles average size was centered at approximately 1.5 μm (Fig. 5(b)).

The nitrogen adsorption/desorption isotherm and the correspondent pores size distribution are given in Fig. S6.

That is a typical type IV isotherm, in which capillary condensation occurred at relative pressures above p/p_0 = 0.8,

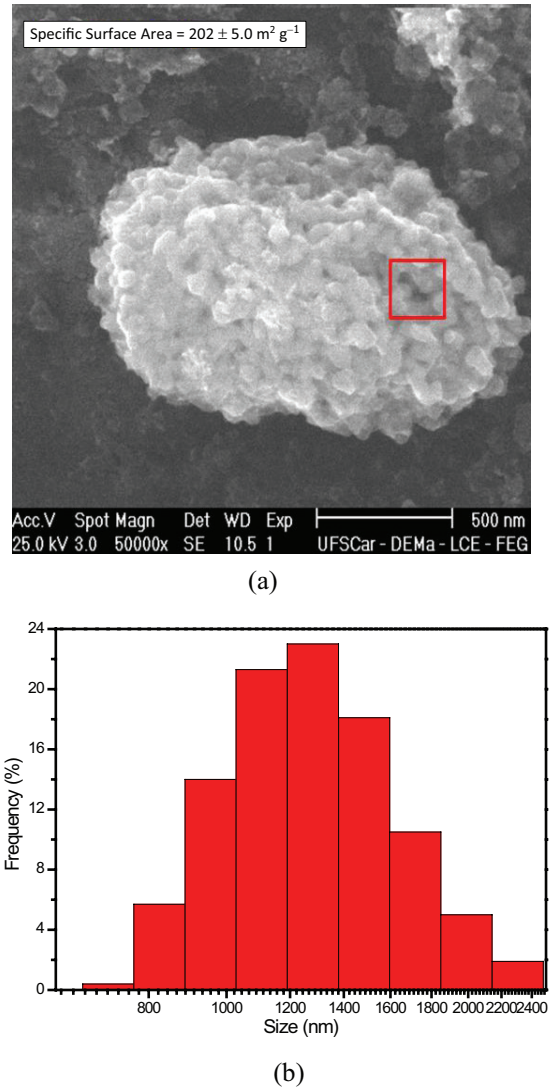

Fig. 5. Fe_3O_4@TiO_2 microparticles: (a) Micrograph (red square – mesopores) and (b) size distribution.

indicating the formation of mesopores and thus explaining the high specific surface area (BET) of 202.0 ± 5.0 m^2 g^{-1} and pores total volume of 0.424 cm^3 g^{-1} [35].

The hysteresis width, besides the pores size distribution, probably indicates bottle-like pores (narrow entrances and large inner volumes). The pores size is centered at approximately 7.0 nm. That mesoporous structure makes it easier for pollutants to diffuse from the solution bulk to the photocatalyst surface.

The IEP was determined as 7.10 (Fig. S7). Therefore, the microparticles surface is positively charged at pH < 7.10 and negatively charged at greater ones.

3.4. Fe_3O_4@TiO_2 photocatalytic activity test

The photocatalytic activity of the microparticles was assessed by degrading AB9. In order to achieve an appropriate condition for the degradation, a 2^2 factorial design was performed.

3.4.1. 2^2 Factorial design

The investigated factors were: (a) Catalyst (microparticles) concentration (0.30 and 1.0 g L^{-1}), levels chosen based on previous studies (not shown here); and (b) Initial pH (3.0 and 8.0). The results of the factorial design can be summarized in the Pareto's chart shown in Fig. S8. One can observe that both effects (catalyst concentration and pH) are statistically significant (within a 95% confidence limit), as well as their interaction. As the catalyst concentration has a positive effect and pH has a negative one, the greatest tested concentration (1.0 g L^{-1}) and the lowest tested pH (3.0) maximize color removal. That reaction conditions were then selected to perform the following experiments.

The catalyst concentration should be always carefully chosen, as two opposing factors influence the photo-degradation: the more catalyst in suspension, the more available catalytic sites for reaction; however, opacity also increases with catalyst concentration, impairing photons to reach inner parts of the suspension.

The pH of a solution influences diffusion, adsorption and dissociation of the dye, catalyst surface charge, and so on. The effect of initial solution pH on the degradation of AB9 by Fe_3O_4@TiO_2 photocatalyst was investigated at initial pH values of 3.0 and 8.0 through of a 2^2 Factorial Design and the results are shown in Table 1.

The degradation efficiency of AB9 was better at initial pH 3.0. This occurs because of the solution pH affects the TiO_2 surface ionic speciation. The pH-dependence of surface charge, which is linked to the point of zero charge (PZC) of the Fe_3O_4@TiO_2 photocatalyst, can be explained by Eqs. (1)–(2).

$$pH < PZC : > TiOH + H^+ \rightleftharpoons TIOH_2^+ \quad (1)$$

$$pH > PZC : > TiOH + OH^- \rightleftharpoons TiO^- + H_2O \quad (2)$$

The PZC value for the prepared Fe_3O_4@TiO_2 photocatalyst is 7.10. Therefore, its surface is positively charged in all acid pH range. The model-pollutant (AB9), when dissolved in water, may be neutral or dissociate to a mono- or divalent anion (pKa_1 = 5.83 and pKa_2 = 6.58) [26]. So, at pH 3.0 the dye is negatively charged. Consequently, the dye molecules could be more favorably adsorbed on the surface of the photocatalyst under acidic conditions, resulting in the increase of photocatalytic degradation efficiency.

Table 1
Factorial design for studying the effect of pH and Fe_3O_4@TiO_2 photocatalyst concentration on the degradation of AB9

Experimental run	Independent variables		Colour removal (%)
	x_1 [a] ($C_{Fe3O4/TiO2}$, g L^{-1})	x_2 [a] (pH)	
1	–1 (0.3)	–1 (3.0)	25.51
2	+1 (1.0)	–1 (3.0)	42.83
3	–1 (0.3)	+1 (8.0)	15.96
4	+1 (1.0)	+1 (8.0)	20.88
5	0 (0.65)	0 (5.5)	13.66
6	0 (0.65)	0 (5.5)	13.24
7	0 (0.65)	0 (5.5)	14.16
8	0 (0.65)	0 (5.5)	15.04

[a] Coded levels.

3.4.2. Color removal kinetics

Kinetic experiments were performed in triplicate during 120 min. Fig. 6 shows the color removal profile. Initially, a pseudo-first-order kinetic regime was established (up to 45 min).

Between 45 and 75 min, no significant color removal was observed. That is possibly due to the formation of recalcitrant intermediates. After those intermediates destruction, the pseudo-first-order kinetic regime was again established with an average $k = (7.6 \pm 1.3) \times 10^{-3}$ min^{-1}, R^2 = 0.981, 95% confidence limit. Approximately 60% of the initial color was removed in 120 min. Within the same elapsed time, only 14% of the color was removed by photolysis.

3.4.3. Reuse cycles

One of the key features a catalyst must have is the ability of being repeatedly used without poisoning or losing its catalytic activity. To check the synthesized photocatalyst performance over time, a series of ten degradation experiments (45 min) were performed in which the same catalyst mass was used after magnetic separation with a new dye solution (50 mL, 25 mg L^{-1}). The results are shown in Fig. 7.

One can observe that, after ten reuse cycles, there was no perceivable photocatalytic activity losses (regarding AB9 degradation), which is a very promising result. The degradation was kept stable at approximately 31%.

4. Conclusions

It was possible to synthesize, without using organic solvents, hematite sub-micro particles with a narrow size distribution centered at 155 nm. A magnetic catalyst with high crystallinity and high specific surface area (202 m^2 g^{-1})

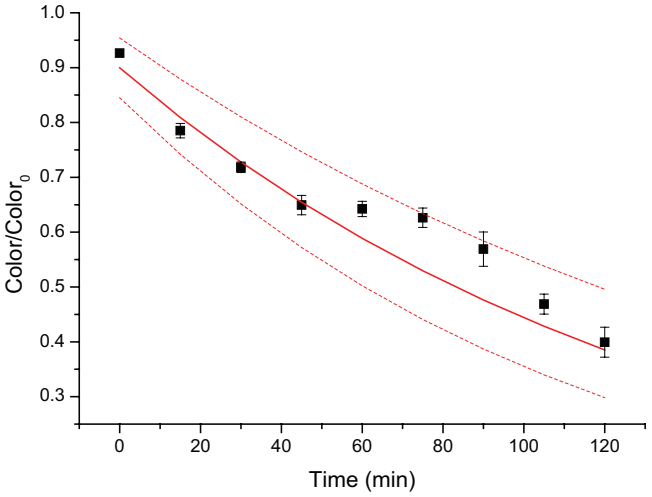

Fig. 6. Color removal profile for 50 mL of a 25 mg L^{-1} aqueous solution of Acid Blue 9. Conditions: initial pH = 3.0; and Fe_3O_4@TiO_2 concentration = 1.0 g L^{-1}.

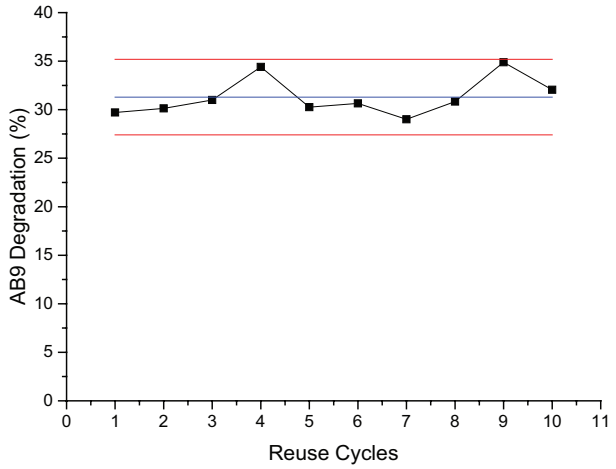

Fig. 7. Photocatalyst (Fe_3O_4@TiO_2) reusability in the Acid Blue 9 (AB9) degradation. The central line shows the experimental points average; the outer ones, two standard deviations (≅95%).

was obtained after coating those particles with TiO_2 and functionalizing them appropriately.

The Fe_3O_4@TiO_2 catalyst presented ferrimagnetic behavior at room temperature and could be easily separated from an aqueous suspension (50 mL, 1.0 g L^{-1}) by an ordinary magnet.

The photocatalytic activity of the sub-micro particles was assessed by degrading a triarylmethane dye when irradiated with UV-Vis light (approximately 60% in 120 min). After ten reuse cycles, the photocatalyst remained active, without any perceivable performance losses.

Acknowledgments

This study was financed in part by the Coordenação de Aperfeiçoamento de Pessoal de Nível Superior – Brasil (CAPES) – Finance Code 001. The authors also wish to thank the Maranhão Research Foundation (FAPEMA) for the acknowledgement of this research through the FAPEMA prize, and Professor Ubirajara Pereira Rodrigues Filho for his invaluable cooperation.

References

[1] D. Mantzavinos, E. Psillakis, Enhancement of biodegradability of industrial wastewaters by chemical oxidation pre-treatment, J. Chem. Technol. Biotechnol., 79 (2004) 431–454.
[2] M.R. Hoffmann, S.T. Martin, W. Choi, D.W. Bahnemann, Environmental applications of semiconductor photocatalysis, Chem. Rev., 95 (1995) 69–96.
[3] O. Legrini, E. Oliveros, A.M. Braun, Photochemical processes for water-treatment, Chem. Rev., 93 (1993) 671–698.
[4] U.M. Nascimento, E.B. Azevedo, Microwaves and their coupling to advanced oxidation processes: enhanced performance in pollutants degradation, J. Environ. Sci. Health, A: Toxic/Haz. Subst. Environ. Eng., 48 (2013) 1056–1072.
[5] A.C. Rodrigues, M. Boroski, N.S. Shimada, J.C.G. Garcia, J. Nozaki, Treatment of paper pulp and paper mill wastewater by coagulation-flocculation followed by heterogeneous photocatalysis, J. Photochem. Photobiol., A., 194 (2008) 1–10.
[6] A.L. Linsebigler, G. Lu, J.T. Yates Jr., Photocatalysis on TiO_2 surfaces: principles, mechanisms, and selected results, Chem. Rev., 95 (1995) 735–758.
[7] L. Ciccotti, L.A.S. Vale, T.L.R. Hewer, R.S. Freire, Fe_3O_4@TiO_2 preparation and catalytic activity in heterogeneous photocatalytic and ozonation processes, Catal. Sci. Technol., 5 (2015) 1143–1152.
[8] K.H. Choi, S.L. Oh, J.H. Jung, J.S. Jung, Efficiently recyclable magnetic core-shell photocatalyst for photocatalytic oxidation of chlorophenol in water, J. Appl. Phys., 111 (2012) 07B504.
[9] S. Xuan, W. Jiang, X. Gong, Y. Hu, Z. Chen, Magnetically separable Fe_3O_4/TiO_2 hollow spheres: fabrication and photocatalytic activity, J. Phys. Chem. C, 113 (2009) 553–558.
[10] S. Kurinobu, K. Tsurusaki, Y. Natui, M. Kimata, M. Hasegawa, Decomposition of pollutants in wastewater using magnetic photocatalyst particles, J. Magn. Magn. Mater., 310 (2007) e1025–e1027.
[11] Z.D. Li, H.L. Wang, X.N. Wei, X.Y. Liu, Y.F. Yang, W.F. Jiang, Preparation and photocatalytic performance of magnetic Fe_3O_4@TiO_2 core-shell microspheres supported by silica aerogels from industrial fly ash, J. Alloys Compd., 659 (2016) 240–247.
[12] Y. Chen, T. Yuan, F. Wang, J. Hu, W. Tu, Magnetically separable Fe_3O_4@TiO_2 nanospheres: preparation and photocatalytic activity, J. Mater. Sci. Mater. Electron., 27 (2016) 9983–9988.
[13] H. Arora, A. Wu, J. Boyle, T. Paunesku, G. Woloschak, Conjugation to Fe_3O_4@TiO_2 nanoparticles increases uptake and nuclear localization of doxorubicin in a drug-resistant ovarian carcinoma model, Int. J. Radiat. Oncol. Biol. Phys., 75 (2009) S564–S565.
[14] Q. He, Z. Zhang, J. Xiong, Y. Xiong, H. Xiao, A novel biomaterial — Fe_3O_4:TiO_2 core-shell nano particle with magnetic performance and high visible light photocatalytic activity, Opt. Mater., 31 (2008) 380–384.
[15] W.J. Chen, P.J. Tsai, Y.C. Chen, Functional Fe_3O_4/TiO_2 core/shell magnetic nanoparticles as photokilling agents for pathogenic bacteria, Small, 4 (2008) 485–491.
[16] X.P. Wu, X. Zhong, Y.Q. Chai, R. Yuan, Electrochemiluminescence acetylcholine biosensor based on biofunctional AMs-AChE-ChO biocomposite and electrodeposited graphene-Au-chitosan nanocomposite, Electrochim. Acta, 147 (2014) 735–742.
[17] W.F. Ma, Y. Zhang, L.L. Li, L.J. You, P. Zhang, Y.T. Zhang, J.M. Li, M. Yu, J. Guo, H.J. Lu, C.C. Wang, Tailor-made magnetic Fe_3O_4@mTiO_2 microspheres with a tunable mesoporous anatase shell for highly selective and effective enrichment of phosphopeptides, ACS Nano, 6 (2012) 3179–3188.
[18] Y. Li, X. Xu, D. Qi, C. Deng, P. Yang, X. Zhang, Novel Fe_3O_4@TiO_2 core-shell microspheres for selective enrichment of phosphopeptides in phosphoproteome analysis, J. Proteome. Res., 7 (2008) 2526–2538.
[19] V. Elhami, A. Karimi, M. Aghbolaghy, Preparation of heterogeneous bio-Fenton catalyst for decolorization of Malachite Green, J. Taiwan. Inst. Chem. Eng., 56 (2015) 154–159.
[20] J. Sánches-martín, J. Beltrán-heredia, M.T. Rodríguez-sánchez, Removal of erioglaucine (Acid Blue 9) with a new coagulant agent from *Acacia mearnsii* tannin extract, Coloration. Technol., 128 (2012) 15–20.
[21] A.R. Khataee, H. Aleboyeh, A. Aleboyeh, Crystallite phase-controlled preparation, characterisation and photocatalytic properties of titanium dioxide nanoparticles, J. Exp. Nanosci., 4 (2009) 121–137.
[22] T. Gessner, U. Mayer In: ULLMANN'S Encyclopedia of Industrial Chemistry. 6th ed., Wiley-VCH: New York, 2001. Triarylmethane and diarylmethane dyes, p. 425–471.
[23] B. Shahmoradi, A. Maleki, K. Byrappa, Photocatalytic degradation of Amaranth and Brilliant Blue FCF dyes using in situ modified tungsten doped TiO_2 hybrid nanoparticles, Catal. Sci. Technol., 1 (2011) 1216–1233.
[24] A.R. Auxilio, P.C. Andrews, P.C. Junk, L. Spiccia, The adsorption behavior of C.I. Acid Blue 9 onto calcined Mg–Al layered double hydroxides, Dyes. Pigm., 81 (2009) 103–112.
[25] J.P. Groten, W. Butler, V.J. Feron, G. Kozianowski, A.C. Renwick, R. Walker, An analysis of the possibility for health implications of joint actions and interactions between food additives, Regul. Toxicol. Pharmacol., 31 (2000) 77–91.

[26] M. Flury, H. Flühler, Tracer characteristics of Brilliant Blue FCF, Soil. Sci. Soc. Am. J., 59 (1995) 22–27.
[27] R. Jain, S. Sikarwar, Photodestruction and COD removal of toxic dye erioglaucine by TiO_2-UV process: influence of operational parameters, Int. J. Phys. Sci., 3 (2008) 299–305.
[28] M.M. Alsolaiman, L. Howard, FD&C blue dye no. 1 and blue nail discoloration: case report, Nutrition, 19 (2003) 395–396.
[29] W.H. Hansen, O.G. Fitzhugh, A.A. Nelson, K.J. Davis, Chronic toxicity of two food colors, Brilliant Blue FCF and Indigotine, Toxicol. Appl. Pharmacol., 8 (1966) 29–36.
[30] M. Ozaki, S. Kratohvil, E. Matijevic, Formation of monodispersed spindle-type hematite particles, J. Colloid. Interface. Sci., 102 (1984) 146–151.
[31] C.M. Flynn Jr., Hydrolysis of inorganic iron (III) salts, Chem. Rev., 84 (1984) 31–41.
[32] L.C. Varanda, M. Jafelicci Jr, P. Tartaj, K.O. Grady, T. Gonzalez-carreño, M.P. Morales, T. Muñoz, C.J. Serna, Structural and magnetic transformation of monodispersed iron oxide particles in a reducing atmosphere, J. Appl. Phys., 92 (2002) 2079–2085.
[33] L.C. Varanda, M. Jafelicci Jr, G.F. Goya, Magnetic properties of spindle-type iron fine particles obtained from hematite, J. Magn. Magn. Mater., 226 (2001) 1933–1935.
[34] P. Gherardi, E. Matijevic, Interactions of precipitated hematite with preformed colloidal titania dispersions, J. Colloid. Interface Sci., 109 (1986) 57–68.
[35] X.W. Lou, L.A. Archer, A general route to nonspherical anatase TiO_2 hollow colloids and magnetic multifunctional particles, Adv. Mater., 20 (2008) 1853–1858.
[36] J. Sun, L. Gao, pH effect on titania-phase transformation of precipitates from titanium tetrachloride solutions, J. Am. Ceram. Soc., 85 (2002) 2382–2384.
[37] H.M. Song, J.M. Ko, J.H. Park, Hybrid photoreactive magnet obtained from Fe_3O_4/TiO_2 composite nanoparticles, Chem. Lett., 38 (2009) 612–613.
[38] IUPAC. The IUPAC Gold Book. Created by Nic M, Jirat J, Kosata B. Updates compiled by Jenkins A, Available at: http://goldbook.iupac.org (Accessed in 20 Aug 2014).
[39] E.P. Barrett, L.G. Joyner, P.P. Halenda, The determination of pore volume and area distributions in porous substances, I. computations from nitrogen isotherms, J. Am. Chem. Soc., 73 (1951) 373–380.
[40] B.D. Cullity, C.D. Graham, Introduction to Magnetic Materials, Addison Wesley: London, 2009.
[41] G.F. Goya, T.S. Berquo, F.C. Fonseca, M.P. Morales, Static and dynamic magnetic properties of spherical magnetite nanoparticles, J. Appl. Phys., 94 (2003) 3520–3528.
[42] B. Barros Neto, I.S. Scarminio, R.E. Bruns. Statistical Design: Chemometrics. Amsterdam: Elsevier B.V; 2006.
[43] L. Cromières, V. Moulin, B. Fourest, E. Giffaut, Physical-chemical characterization of the colloidal hematite/water interface: experimentation and modeling, Coll. Surf., A., 202 (2002) 101–115.
[44] M. Baalousha, Aggregation and disaggregation of iron oxide nanoparticles: influence of particle concentration, pH and natural organic matter, Sci., Total. Environ., 407 (2009) 2093–2101.
[45] S. Al-sayari, A.F. Carley, S.H. Taylor, G.J. Hutching, Au/ZnO and Au/Fe_2O_3 catalysts for CO oxidation at ambient temperature: comments on the effect of synthesis conditions on the preparation of high activity catalysts prepared by coprecipitation, Top. Catal., 44 (2007) 123–128.
[46] Z. Zhong, J. Ho, J. Teo, S. Shen, A. Gedanken, Synthesis of porous α-Fe_2O_3 nanorods and deposition of very small gold particles in the pores for catalytic oxidation of CO, Chem. Mater., 19 (2007) 4776–4782.
[47] A.H. Lu, E.L. Slabas, F. Schuth, Magnetic nanoparticles: synthesis, protection, functionalization, and application, Angew. Chem. Int. Ed. Engl., 46 (2007) 1222–1244.
[48] J.P. Jolivet, De la solution à l'oxyde: condensation des cations en solution aqueuse. Chimie de surface des oxyde, InterÉditions/CNRS Éditions, Paris, 1994.
[49] C.L. Zhu, M.L. Zhang, Y.J. Qiao, G. Xiao, F. Zhang, Y.J. Che, Fe_3O_4/TiO_2 core/shell nanotubes: synthesis and magnetic and electromagnetic wave absorption characteristics, J. Phys. Chem. C, 14 (2010) 16229–16235.
[50] H. Lee, E. Lee, D.K. Kim, N.K. Jang, Y.Y. Jeong, S. Jon, Antibiofouling polymer-coated superparamagnetic iron oxide nanoparticles as potential magnetic resonance contrast agents for in vivo cancer imaging, J. Am. Chem. Soc., 128 (2006) 7383–7389.
[51] T. Sugimoto, K. Sakata, A. Muramatsu, Formation mechanism of monodisperse pseudocubic α-Fe_2O_3 particles from condensed ferric hydroxide gel, J. Colloid. Interface Sci., 159 (1993) 372–382.

Supplementary material

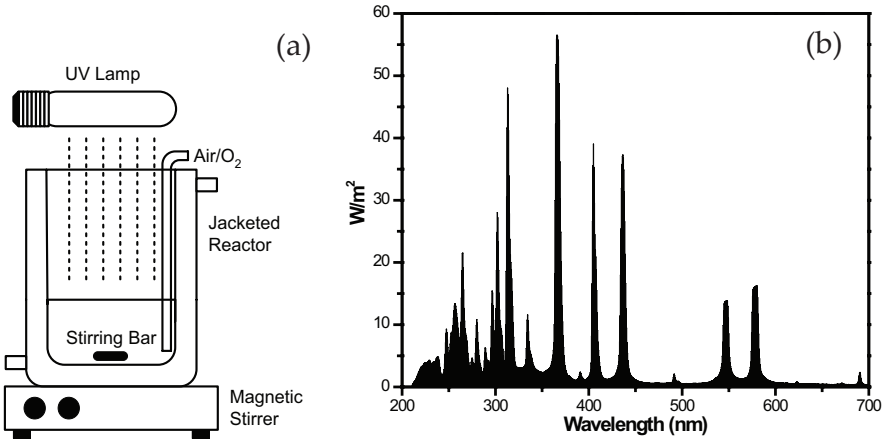

Fig. S1. Apparatus: (a) cylindrical borosilicate reactor (250 mL, 25°C ± 2°C) scheme; (b) medium-pressure mercury-vapor lamp spectrum.

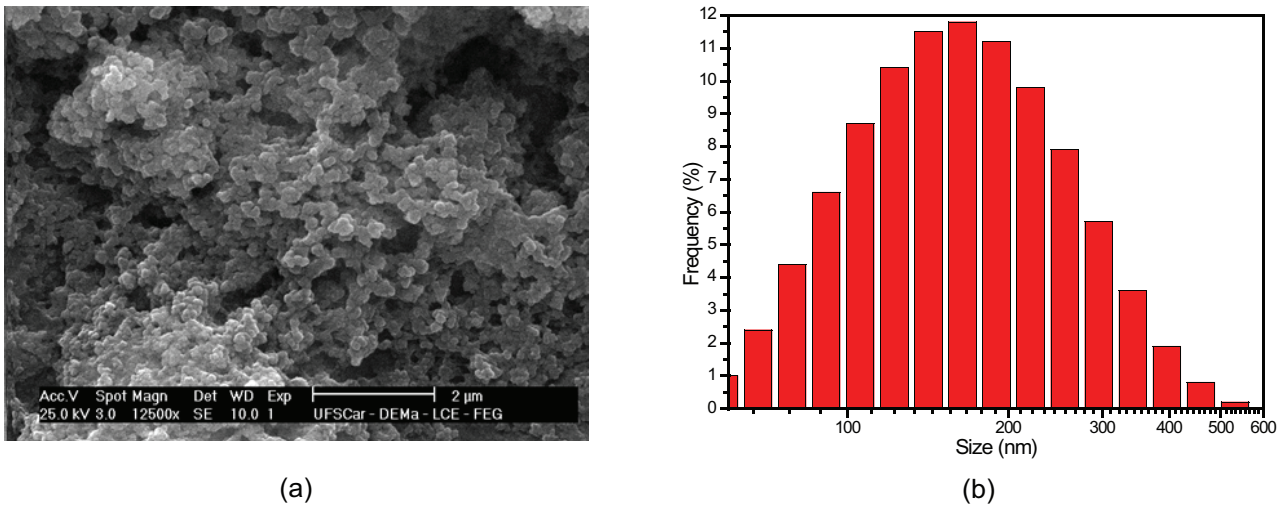

Fig. S2. Hematite sub-micro particles: (a) micrograph of particles agglomeration; (b) size distribution.

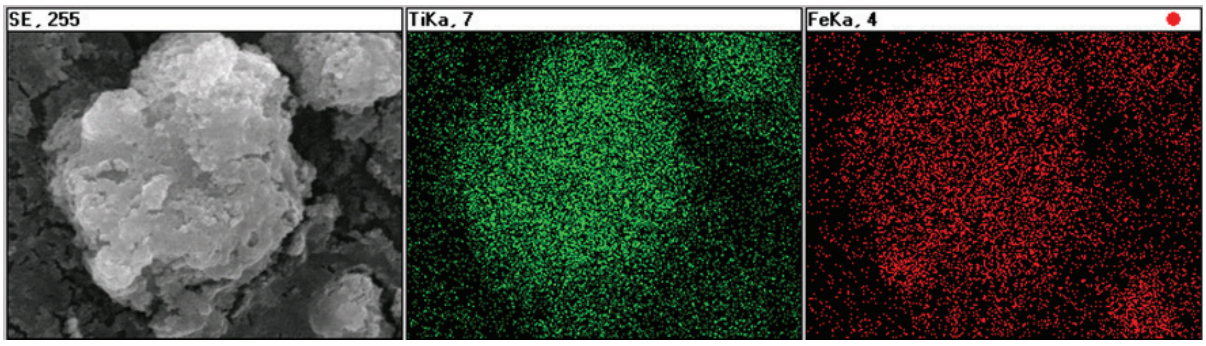

Fig. S3. EDS mapping: (a) Micrograph of Fe_2O_3@TiO_2 microparticles; (b) Titanium distribution and (c) Iron distribution.

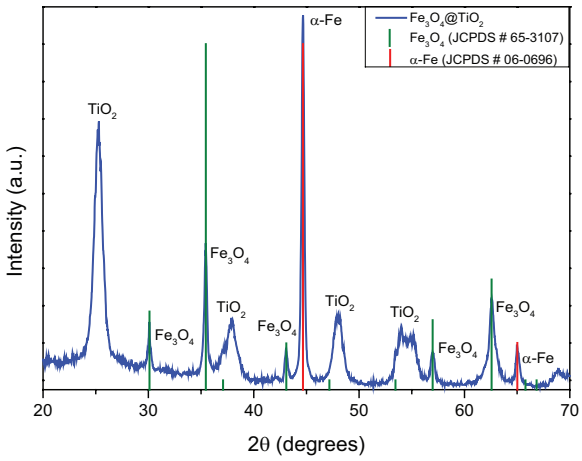

Fig. S4. Diffractogram of the synthesized Fe_3O_4@TiO_2 microparticles. Magnetization conditions: 400°C for 1 h under reducing atmosphere (H_2).

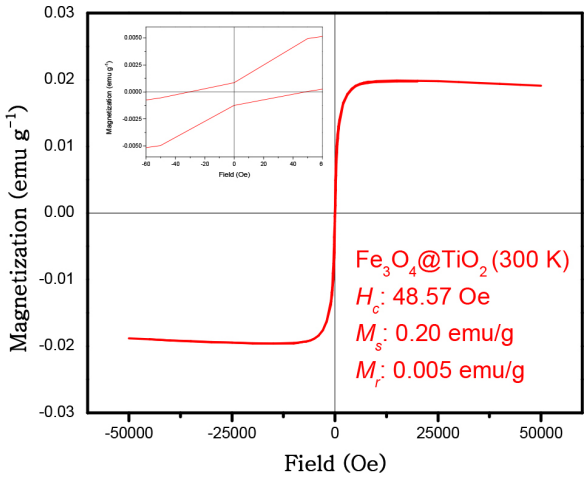

Fig. S5. Fe_3O_4@TiO_2 microparticles: magnetization hysteresis curves (insert – coercivity).

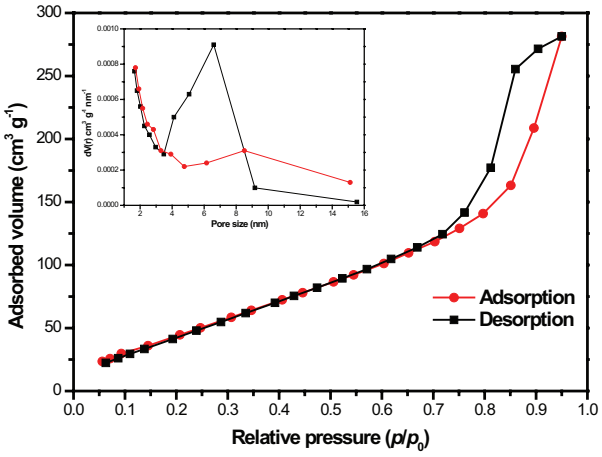

Fig. S6. Fe_3O_4@TiO_2 microparticles: Nitrogen adsorption/desorption isotherm (insert – pores size distribution).

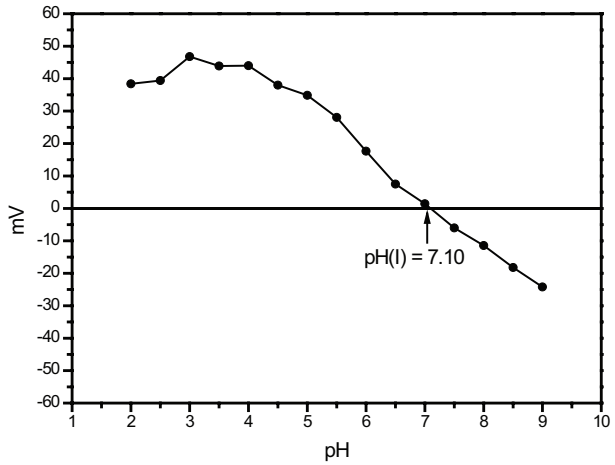

Fig. S7. Fe_3O_4@TiO_2 microparticles: isoelectric point.

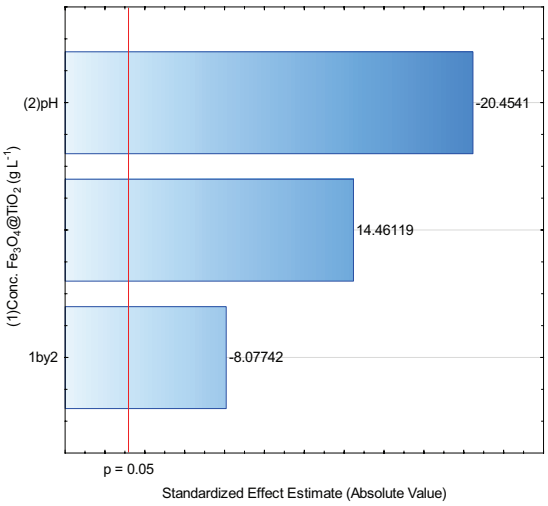

Fig. S8. Pareto's chart showing the standardized effects estimates for: photocatalyst (Fe_3O_4@TiO_2) concentration, initial pH and their interaction.